Convection-Enhanced Delivery of AAV Vector in Parkinsonian Monkeys; *In Vivo* Detection of Gene Expression and Restoration of Dopaminergic Function Using Pro-drug Approach

Krys S. Bankiewicz,*,† Jamie L. Eberling,†,‡ Malgorzata Kohutnicka,*,1 William Jagust,†,‡ Phillip Pivirotto,* John Bringas,* Janet Cunningham,§ Thomas F. Budinger,† and Judith Harvey-White*

*Molecular Therapeutics Section, LMMN, NINDS, Bethesda, Maryland 20892; †Center for Functional Imaging, Lawrence Berkeley Laboratory, University of California, Berkeley, California; §Avigen, Inc., Alameda, California; and ‡Department of Neurology, University of California, Davis, California

Received December 1, 1999; accepted February 10, 2000

Using an approach that combines gene therapy with aromatic L-amino acid decarboxylase (AADC) gene and a pro-drug (L-dopa), dopamine, the neurotransmitter involved in Parkinson's disease, can be synthesized and regulated. Striatal neurons infected with the AADC gene by an adeno-associated viral vector can convert peripheral L-dopa to dopamine and may therefore provide a buffer for unmetabolized L-dopa. This approach to treating Parkinson's disease may reduce the need for L-dopa/carbidopa, thus providing a better clinical response with fewer side effects. In addition, the imbalance in dopamine production between the nigrostriatal and mesolimbic dopaminergic systems can be corrected by using AADC gene delivery to the striatum. We have also demonstrated that a fundamental obstacle in the gene therapy approach to the central nervous system, i.e., the ability to deliver viral vectors in sufficient quantities to the whole brain, can be overcome by using convection-enhanced delivery. Finally, this study demonstrates that positron emission tomography and the AADC tracer, 6-[^{18}F]fluoro-L-*m*-tyrosine, can be used to monitor gene therapy *in vivo*. Our therapeutic approach has the potential to restore dopamine production, even late in the disease process, at levels that can be maintained during continued nigrostriatal degeneration. © 2000 Academic Press

INTRODUCTION

An emerging new technology based on genetically engineering viral vectors that can insert genes into the cells of living organisms may play a significant role in treating disorders of the central nervous system (CNS) (9, 10, 20–22). Since the brain is highly specialized, neurodegenerative disease process affects focal regions of the brain and spinal cord. Preventive and/or treatment strategies will need to be targeted to only the diseased regions of the brain, without affecting other regions. Administration of therapeutic genes specifically to the disease-affected regions of the brain may be more beneficial than current treatment strategies, which are largely based on systemically administering small molecules or proteins. The latter can result not only in peripheral side effects but also in CNS side effects, since the drugs can affect both targeted and nontargeted brain sites. In addition, many therapeutic agents are prevented from entering the brain by the blood–brain barrier (BBB). For these reasons, many otherwise potentially useful proteins such as trophic factors, can not be administered systemically since they have peripheral and central side effects and cannot pass the BBB (23).

Parkinson's disease is a good example of a focal brain disorder in which slow degeneration of dopamine-producing neurons, mostly in the nigrostriatal pathway, results in neurological signs. By the time these signs are evident, at least 60–80% of dopamine is lost both in the substantia nigra and in the caudate and putamen, where dopamine interacts with postsynaptic dopaminergic receptors. Since dopamine cannot cross the BBB, the current treatment for Parkinson's disease is a replacement strategy in which the dopamine precursor, L-dopa, which can pass the BBB, is given orally several times a day. The biosynthetic pathway for dopamine contains two critical enzymes, tyrosine hydroxylase (TH), which converts the amino acid tyrosine to dopa, and aromatic-amino-dopadecarboxylase (AADC), which decarboxylates dopa to dopamine. Administration of L-dopa bypasses the TH step, and L-dopa is converted into dopamine by AADC. Typically, L-dopa is given together with carbidopa, the peripheral inhibitor of AADC, to reduce the catabolism of L-dopa peripherally, thus prolonging its plasma and brain levels (5, 27,

---

29). Unfortunately, this treatment strategy is of limited benefit because AADC levels decrease with the progression of the disease, thereby preventing the conversion of L-dopa into dopamine in sufficient quantities (33). Thus, while L-dopa/carbidopa treatment works well in the early stages of the disease, larger doses of the drug are required as the disease progresses and effectiveness declines, leaving the patients with reduced therapeutic benefits and increased side effects (31, 34).

Our experiments were designed to determine if AADC delivery by gene transfer directly into targeted brain sites together with the systemic administration of L-dopa as a pro-drug can restore dopaminergic activity in (1-methyl-4-phenyl-1,2,3,6-tetrahydropyridine (MPTP)-treated monkeys. A critical issue with brain-targeted gene therapy is the difficulty of measuring transgene expression *in vivo.* Here, *in vivo* gene expression was measured using positron emission tomography (PET) and the AADC tracer 6-[18F]fluoro-L-*m*-tyrosine (FMT) (17, 18). Detection of gene expression by PET is limited by extent of gene transfer. In our first attempt to use AADC vector with pro-drug administration to induce recovery of dopaminergic activity we observed very limited signal that appeared to correlate with small regions of gene transfer (11).

This study further addressed the essential aspects of gene transfer, such as the delivery of viral vectors to large anatomical brain structures using the convection-enhanced delivery (CED) method. We showed that adeno-associated viral vectors (AAV) can be distributed in the brain using CED in a rat (7) and a primate brain (3, 4, 11). In this study AAV was delivered to the caudate and putamen using CED to determine if these vectors could be distributed in homogenous tissue concentrations over a large region of the monkey striatum.

MATERIALS AND METHODS

Experimental Design

The experimental design included unilateral intra-carotid artery (ICA) plus iv administration of the dopaminergic toxin MPTP to four monkeys followed by baseline magnetic resonance imaging (MRI) and PET scans. The combination of unilateral ICA and iv MPTP administration produces a nearly complete dopaminergic lesion on the side of the carotid artery (CA) infusion (ipsilateral side) and a partial lesion on the other side of the brain (contralateral side) (1, 2, 12, 13). CED of either AAV with reporter (LacZ) ($n = 2$) or therapeutic genes (AADC) ($n = 2$) to the ipsilateral striatum was subsequently performed. PET scans were performed 7–8 weeks after gene delivery and followed 1 week later by biochemical and histological examinations. Prior to euthanasia, animals were treated with L-dopa/

carbidopa to determine the biochemical consequences of AADC gene delivery.

Experimental Subjects

The protocol was reviewed and approved by the Institutional Animal Care and Use Committee. Rhesus monkeys ($n = 4$, 3–5 kg) were lesioned by infusing 2.5–3.5 mg of MPTP–HCl through the right internal carotid artery (referred to as the ipsilateral side) followed by four iv doses of 0.3 mg/kg of MPTP–HCl (referred to as the contralateral side) until a stable, overlesioned hemiparkinsonian syndrome was achieved. Animals were clinically evaluated once a week using a clinical rating scale and activity monitoring for 5 months prior to surgery. This model mimics the biochemical and histopathological changes seen in advanced stages of idiopathic Parkinson's disease. Following MPTP administration, animals developed clinical signs of Parkinson's disease manifested by general slowness, bradykinesia, rigidity, balance disturbances, and flexed posture. The left arm was less frequently used than the right in all monkeys; all showed signs of tremor. Using the parkinsonian clinical rating scale, all monkeys had moderate-to-severe stable parkinsonian scores (23 ± 1.7, 23 ± 1.2, 24 ± 1.7, 19 ± 3) during the 5-month post-MPTP period. Only reliable baseline clinical parkinsonian assessment, and not L-dopa-induced evaluation, was possible in these monkeys since they failed to interact well with the raters. For that reason, no attempt was made to study clinical responses to peripheral L-dopa/carbidopa administration because this type of evaluation requires a large number of animals that interact well with the raters. Following intrastriatal AAV administration, animals were assessed for any signs of abnormal behavior and were observed and rated by the veterinary technicians twice a day. All monkeys recovered from the surgery within 2 h and were able to maintain themselves, including feeding and grooming.

Magnetic Resonance Imaging

Visualization of the target site is crucial for precise placement of virus within the caudate nucleus or putamen. Stereotactic procedures combined with MRI were used to accurately place the cannula within the desired targeted structures (37). All animals were scanned before surgery to generate accurate stereotactic coordinates of the target implant sites for each animal. The same fiducial markers that are used for PET scanning were placed on the frame for coregistration of MRI and PET images. During the scanning procedure, animals were sedated using a mixture of ketamine (Ketaset, 7 mg/kg, im) and xylazine (Rompun, 3 mg/kg, im). Animals were placed in an MRI-compatible stereotactic frame, earbar and eyebar measurements were recorded, and an iv line was established. Sixty coronal images (1 mm) and 15 sagittal images (3 mm) were taken using a GE Signa 1.5-T

machine. Magnetic resonance images were T_1-weighted and obtained in three planes using a spoil grass sequence with a repetition time (T_R) = 700 ms, an echo time (T_E) = 20 ms, and a flip angle of 30°. The field of view was 15 cm, with a 192 matrix and a 2 NEX (number of averages per signal information). Baseline scanning time was approximately 20 min. Rostrocaudal and mediolateral distribution of a targeted structure (e.g., caudate nucleus) was determined using the coronal MR images. Surgical coordinates were determined from magnified coronal images (1.5×) of the caudate nucleus and putamen.

Positron Emission Tomography

All four animals received two PET scans; a baseline scan 3 months after MPTP administration and a second scan 7–8 weeks after infusion with either AAV–AADC or AAV–LacZ. The PET studies were performed on the PET-600 system, a single-slice tomograph with a resolution of 2.6 mm in-plane and an adjustable axial resolution that was increased from 6 to 3 mm for the current study by decreasing the shielding gap. The characteristics of this tomograph have been described previously (36). Monkeys were intubated and anesthetized with isoflurane, placed in a stereotaxic frame, and positioned in the PET scanner so as to image a coronal brain slice passing through the striatum. Animals were positioned in the same way for each study using the anterior–posterior scales on the stereotaxic frame and a laser light connected to the tomograph. After being positioned in the scanner, a 5-min transmission scan was obtained to correct for photon attenuation and to check the positioning of the animal. The monkeys were then injected with 10–15 mCi of FMT and imaging was begun. Imaging continued for 60 min, at which time the monkey was repositioned so as to image a second slice 6 mm caudal to the first. The PET and MRI data sets were coregistered and regions of interest (ROI) were drawn for the striatum in the contralateral hemisphere (the side opposite the ICA MPTP infusion) on PET data collected at 50 to 60 min (slice 1) and from 65 to 75 min (slice 2) with reference to the MRI. Mirror images of the ROI were created in the ipsilateral hemisphere (side of MPTP infusion) and radioactivity counts (cm^2/s) were determined for each ROI. Striatal counts were averaged over the two slices for each study. FMT uptake asymmetry ratios were calculated for each animal at each time point by subtracting the counts for the ipsilateral (lesioned) striatum from the counts for the contralateral striatum and dividing by the average counts for the ipsilateral and contralateral striata. In order to reduce between-animal variability in asymmetry ratios, a change score was calculated by subtracting the asymmetry ratio for the second PET study from the asymmetry ratio for the baseline study for each animal.

Surgical Procedures

Preparation of loading lines. In the surgery room, a sterile field was created to prepare the infusion system. Infusion cannulae were flushed with saline to assess the integrity between the needle and the tubing interface. Sterile infusion cannulae and loading lines were connected using the appropriate fittings with extreme caution taken to prevent the collection of air bubbles in the system. Oil infusion lines were prepared and 1-ml gas-tight Hamilton syringes filled with oil were attached to a Harvard infusion pump. Six infusion cannulae were fitted onto holders (three cannulae per holder) and mounted onto a stereotactic tower. Following the union of the oil and loading lines, the needle cannulae were primed with AAV and the infusion system was transferred to the surgery table. Initial infusion rates were set at 0.1 μl/min, the lines visually inspected to ensure a smooth flow of fluid through the system, and the cannulae manually lowered to their target sites.

Cannula design. The cannula system consisted of three components: (i) sterile infusion cannula, (ii) sterile loading line housing AAV–DDC or AAV–LacZ, and (iii) a nonsterile infusion line containing olive oil. The infusion cannula consisted of 27-gauge needles (o.d., .03 in.; i.d., .06 in; Terumo Corp., Elkton, MD) fitted with fused silica (o.d., .016 in; i.d., .008 in.; Polymicro Technologies, Phoenix, AZ) and placed in Teflon tubing (.03 in. i.d.; Upchurch Scientific, Seattle, WA) such that the distal tip of the silica extended approximately 15 mm out of the tubing. The needle was secured into the tubing using superglue and the system was checked for leaks prior to use. At the proximal end of the tubing, a Tefzel fitting and ferrule were attached to connect the adjacent loading line. Loading and infusion lines consisted of 50-cm sections of Teflon tubing (o.d., .062 in.; i.d., .03 in.) fitted with Tefzel 1/16-in. ferrules, unions, and male Luer-lock adapters (Upchurch Scientific, Oak Harbor, WA) at the distal ends. The sterile loading lines accommodated up to a 1000-μl volume and were primed with saline prior to use.

Intrastriatal Infusion of AAV

The animals were initially sedated with Ketamine (Ketaset; 10 mg/kg, im), intubated, and prepped for surgery. A venous line was established using a 22-gauge catheter positioned in the cephalic or saphenous vein to deliver isotonic fluids at 5–10 ml/kg/h. Isoflurane (Aerrane, Omeda PPD, Inc., Liberty, NJ) was delivered at 1–3% until the animal maintained a stable plane of anesthesia. The head was placed in an MRI-compatible stereotactic frame according to preset values attained during a baseline MRI scan. Vital signs were monitored. A sterile field was created and a midline incision performed through the skin, muscle, and fascia using electrocautery (Surgistat Electrosurgery,

Valleylab, Inc., Boulder, CO). Gentle retraction of fascia and muscle allowed for cranial exposure over cortical entry sites. A unilateral craniotomy was performed using a Dremel dental drill to expose a 3 cm $\times$ 2-cm area of dura mater above the target sites. Multiple needle cannulae attached to a holder were stereotactically guided to striatal target sites. Two sites in caudate and four sites in each putamen were targeted. Thirty microliters of AAV was infused in each site at 0.1 and 0.2 (μl/min for 60 min followed by 30-min infusion at 0.4 μl/min. AAV–AADC (3.6×10^{11}) or AAV–LacZ (1.5×10^{11}) (total particles) was administered into each monkey. Approximately 15 min following infusion, the cannulae assembly was raised at a rate of 1/mm/min until it was out of the cortex. The cortex was rinsed with saline, bone margins were trimmed with ronguers, and the wound site was closed in anatomical layers. Animals were monitored for full recovery from anesthesia, placed in their home cages, and clinically observed (2$\times$/day) for 5 days following surgery. Total neurosurgery time was 4.5 h per animal.

AAV Production

The HEK 293 cell line was cultured in complete DMEM (BioWhittaker) containing 4.5 g/l glucose, 10% heat-inactivated fetal calf serum (FCS), and 2 mM glutamine at 37°C in 5% CO_2 in air. Forty T225 flasks were seeded with 2.5×10^6 cells each and grown for 3 days prior to transfection to 70–80% confluency (approximately 1.5×10^7 cells per flask). The transfection and purification methods (16, 30) were employed for AAV production, with minor modifications. The vector production process involved cotransfection of HEK 293 cells with 20 μg of each of the following three plasmids per flask: the AAV–AADC plasmid, the AAV helper plasmid (pHLP19, containing the AAV rep and cap genes), and the adenovirus helper plasmid (pladeno-5, previously known as pVAE2AE4-2 and composed of the E2A, E4, and VA RNA genes derived from purified adenovirus-2), using the calcium phosphate method for a period of 6 h. After transfection, the media were replaced and the cells were harvested 3 days later. Cell pellets were then subjected to three cycles of freeze–thaw lysis (alternating between dry ice–ethanol and 37°C baths with intermittent vortexing). The cell debris was removed by centrifugation ($10,000g$ for 15 min). Supernatant was centrifuged a second time to remove any remaining turbidity and subsequently treated with BenzonaseR at 37°C for 1 h to reduce contaminating cellular DNA. Following incubation, the supernatant was made and placed on ice for 1 h. The resulting precipitate was removed by centrifugation ($10,000g$ for 15 min) and discarded. The supernatant was then made (10% in PEG(8000)) and was placed on ice for 3 h. Precipitate was collected by centrifugation ($3000g$ for 30 min) and resuspended in 4 ml of 50 mM

Na–Hepes, 0.15 M NaCl, 25 mM EDTA (pH 8.0) per 20 T225 flasks. Solid CsCl was added to produce a density of 1.4 g/ml and the sample was centrifuged at $150,000g$ for 24 h in a Beckman T170 rotor. AAV-containing fractions were pooled, adjusted to a density of 1.4 g/ml CsCl, and centrifuged at $350,000g$ for 16 h in a Beckman NVT65 rotor. The fractions containing AAV were then concentrated and diafiltered against excipient buffer (5% sorbitol in PBS). The titer of the purified AAV–AADC vector was determined using quantitative dot blot analysis and vector stocks were stored at −80°C.

Construction of AAV–AADC Plasmid

A 1.5-kb *Bam*HI/*Pvu*II human AADC cDNA (courtesy of Dr. Keiya Ozawa, Jichi Medical School, Tochigi, Japan) was cloned into the AAV expression casette pV4.1c at *Bam*HI/*Hin*dII sites. The expression casette contained a CMV promoter, a chimeric intron composed of a CMV splice donor and a human globin splice acceptor site, human growth hormone polyadenylation sequence, and flanking AAV ITRs (inverted terminal repeats) (39).

Histological Procedures

Animals were deeply anesthetized with sodium pentobarbital (25 mg/kg iv) and sacrificed 8 weeks following AAV administration and 1 week following postsurgical PET scans. On the day of sacrifice, the animals were treated with L-dopa/carbidopa preparation (Sinemet 250/25). The brains were removed 30–45 min following Sinemet administration, placed in the brain matrix, and sectioned coronally into 3- to 6-mm slices. One 3-mm-thick striatal brain slice from each monkey was immediately frozen in −70°C isopenthane and stored frozen for biochemical and histological analysis. The remaining 6-mm-thick slices were postfixed in formalin for 72 h, washed in PBS for 12 h, and adjusted in an ascending sucrose gradient (10–20–30%) and frozen.

The formalin-fixed brain slices were cut into 30-μm-thick coronal sections in a cryostat. Sections were collected in series starting at the level of the rostral tip of the caudate nucleus all the way caudally to the level of the substantia nigra. Each section was saved and kept in antifreeze solution at −70°C. Frozen blocks were partially sectioned in the cryostat at 18 μm before tissue punches were taken. Following tissue punching the remaining blocks were sectioned in the cryostat. Sections were postfixed in formalin for 15 min and processed for immunocytochemistry and H & E staining. Serial sections were stained for tyrosine hydroxylase (TH), ADDC, or LacZ immunoreactivity (IR). Every 12th section was washed in phosphate-buffered saline (PBS) and incubated in 3% H_2O_2 for 20 min to block the endogenous peroxidase activity. After being

washed in PBS, the sections were incubated in blocking solution (10% normal horse serum for TH or 10% normal goat serum for ADDC and β-gal and 0.1% Triton-X 100 in PBS) for 30 min, followed by incubation in primary antibody solution—TH (mouse monoclonal, Chemicon, 1:1000), ADDC (rabbit polyclonal, Chemicon, 1:2000), or β-gal (rabbit polyclonal, Cortex Biochem, 1:5000) for 24 h. The sections were then incubated for 1 h in biotinylated anti-mouse IgG secondary antibody for TH or anti-rabbit IgG secondary antibody for ADDC and β-gal (Vector Labs, 1:300). The antibody binding was visualized with streptavidin horseradish peroxidase (Vector Labs, 1:300) and DAB chromogen with nickel (Vector Labs). Sections were then coverslipped and examined under a light microscope.

Stereological Analysis of AAV–AADC-Infected Cells

Quantitative estimates of the total number of AAV-infected cells within the caudate nucleus, putamen, and globus pallidus were determined using an optical dissector procedure. This system consisted of a computer-assisted image analysis system, including a Leitz Otholux II microscope hard-coupled to a Prior H128 computer-controlled x-y-z motorized stage, a high sensitivity Sony 3CCD video camera system (Sony, Japan), and a Macintosh G-3 computer. All analyses were performed using NeuroZoom software (La Jolla, CA). Prior to each series of measurements, the instrument was calibrated. The region of positive neurons in the caudate, putamen, and globus pallidus was outlined at low magnification (2.5× objective). Because of the diffuse presence of AAV-infected cells within the striatum, 1% of the outlined region was measured with a systematic random design of dissector counting frames (1505 μm2) using a 63× plan-neofluar immersion objective with a 0.95 numerical aperture. Based on pilot experiments, at least four sections were sampled. By using the dissector principle, up to 200 cells were sampled by optical scanning by using uniform, systematic, and random design procedures for all measurements. The average thickness of the sections was measured at 23 μm. Once the top of the section was in focus, the z-plane was lowered 1–2 μm. Counts were then made while focusing down through three 5-μm-thick dissectors. Care was taken to ensure that the bottom forbidden plane was never included in the analysis. The volumes of the structures were calculated according to the procedure of Cavalieri (6). The total number of positive cells in the examined structures was calculated by using the formula $N = N_V \times V_S$, where N_V is the numerical density and V_S is the volume of the structure (38).

Biochemical Analysis

Brain regions were removed from fresh frozen blocks using a micropuncher in order to evaluate tissue levels of L-dopa and dopamine metabolites and activity of AADC. Frozen micropunches were collected and homogenized by ultrasonic processing in 300 μl of 0.1 M perchloric acid (Fisher Scientific) containing 1% ethanol and 0.02% EDTA (Fisher Scientific). Fifty microliters of the homogenate was removed for protein analysis (BCA Protein Assay Kit Pierce), and the remainder centrifuged in a microcentrifuge for 1.5 min at maximum speed. Thirty to fifty microliters of the homogenate was used for catecholamine analysis by HPLC using an Ultrasphere C-18 ion pair, 5 μ, 4.6 × 250-mm column (Beckman 235329); a Waters 717 plus autosampler at 4°C, Waters 510 pump at 0.9 ml/min, and amperometric electrochemical detector (Decade) set at Eox. 0.82 V. The column and detector cell were set at 31°C. The mobile phase contained 2 l HPLC grade water, 2.2 g 1-heptanesulfonic acid, sodium salt (Fisher Scientific), 0.17 g EDTA, 12 ml triethylamine (Fisher Scientific), pH adjusted to 2.5 with 8 ml 85% phosphoric acid (Fisher Scientific), and 60 ml acetonitrile (J. T. Baker). The detector output was recorded and analyzed with the Waters Millennium 32 Chromatography Manager.

Tissue (10 mg/ml) was homogenized in 50 mM phosphate buffer (pH 7.4) containing 0.04 mM pyridoxyl phosphate (a AADC cofactor) and 0.2 mM pargyline. Samples were preincubated at 37°C for 5 min and the reaction was initiated by the addition of L-dopa (final concentration, 100 μM). Incubations were carried out for 20 min and the reaction was stopped by addition of
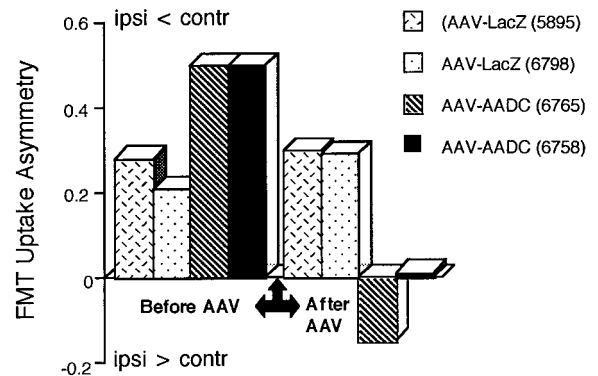

FIG. 1. Asymmetry in striatal 6-[18F]fluoro-L-m-tyrosine (FMT) uptake. Baseline positron emission tomography studies showed that MPTP almost completely reduced dopaminergic activity in the ipsilateral striatum with respect to the partially lesioned contralateral striatum. Baseline FMT asymmetry ratios (contralateral radioactivity counts minus ipsilateral activity counts divided by the average counts for both striata) were positive in all four monkeys. Little or no change in asymmetry ratios were seen in the AAV–LacZ-treated monkeys, while the AAV–DDC-treated monkeys showed little difference between ipsilateral and contralateral striata, indicating increased AADC activity in the ipsilateral striatum. In fact, FMT uptake in the ipsilateral striatum actually exceeded contralateral striatal uptake in one monkey (No. 6765) following AAV–AADC administration.
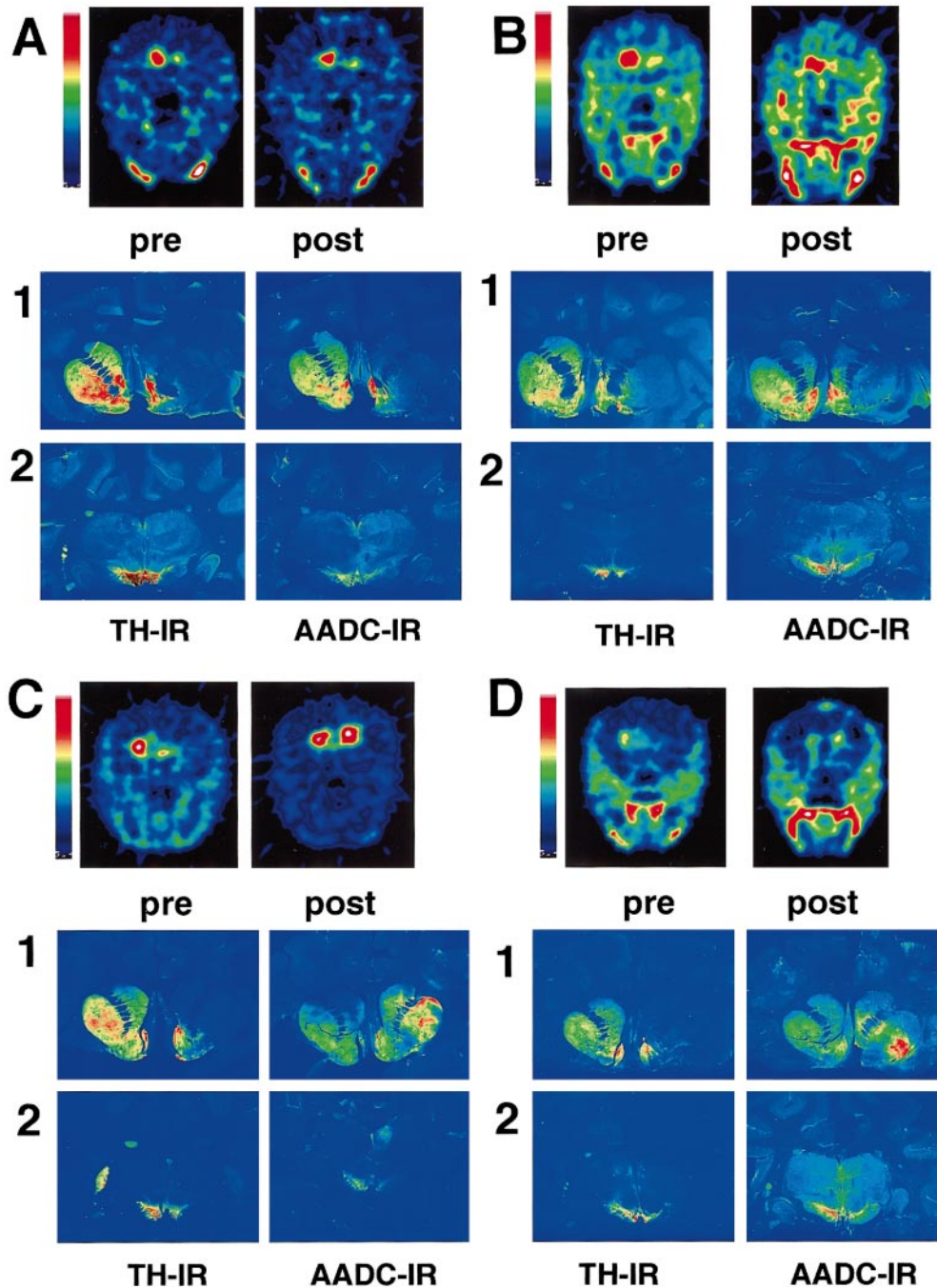
FIG. 2. Positron emission tomography studies of FMT uptake in the striatum before and after AAV administration. AAV–LacZ-treated monkeys, A-6798, B-5895; AAV–DDC-treated monkeys, C-6765, D-6758. Histological representation of the striatum (1) and substantia nigra (2) processed for TH and AADC immunoreactivity (IR). FMT uptake was negligible in the ipsilateral striatum in all monkeys prior to AAV administration. AAV–LacZ-treated monkeys (A, B) showed little change in ipsilateral FMT uptake following AAV administration. On postmortem examination, TH- and AADC-IR were markedly reduced in these monkeys. AAV–AADC-treated animals showed a dramatic increase in ipsilateral FMT uptake that exceeded uptake in the contralateral striatum in monkey 6765 (C). AADC-IR, but not TH-IR, was restored on the ipsilateral side by AAV–AADC administration. Note the profound depletion of dopaminergic cells in the ipsilateral substantia nigra in all monkeys.
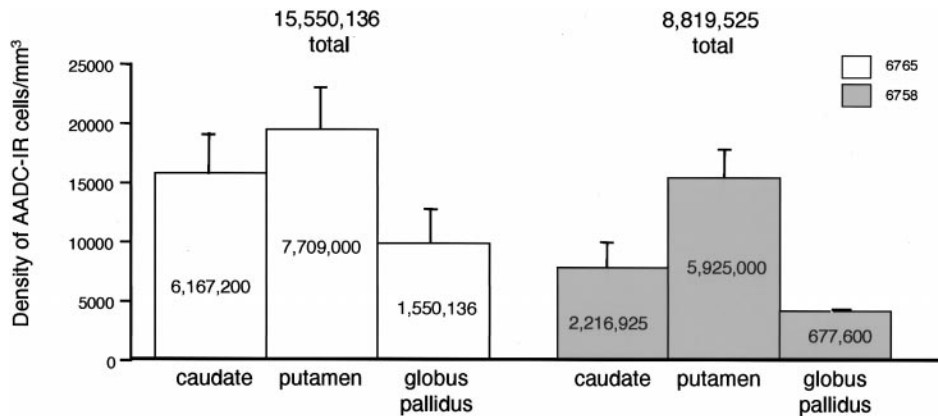
FIG. 3. Quantification of density and number of AAV-infected cells in the caudate, putamen, and globus pallidus of AAV–AADC-treated monkeys.

0.02 ml concentrated perchloric acid. After centrifugation, the supernatant dopamine concentration was determined using HPLC with electrochemical detection. Protein concentration in the tissue pellet was determined using the BCA Protein Assay Kit (Pierce). Results were expressed as nanomolar per hour per milligram of protein. Tissue from cortex and striatum of three normal rhesus monkeys was obtained and processed with AAV-treated monkey tissue samples. Normal AADC levels in the monkey striatum are 56 nmol/hr/mg protein ($\pm$12 SD).

RESULTS

As expected, at baseline all four monkeys showed greater FMT uptake in the contralateral than in the ipsilateral striatum, which had negligible uptake. Previous work from our laboratory has shown relatively symmetrical striatal FMT uptake in unlesioned monkeys (13). Following AAV administration, at the time of the second PET study, the AAV–AADC-treated monkeys had increased FMT uptake in the ipsilateral striatum, while the AAV–LacZ-treated animals showed little change from baseline (Figs. 1 and 2). AAV–LacZ-treated monkeys had greater contralateral FMT uptake at both time points. As shown in Fig. 2, FMT in areas outside of the striatum was fairly symmetrical, although most of this uptake was outside of the brain.

To confirm the PET results, histological assessment of the brains was performed. TH-immunoreactive staining revealed markedly reduced nigrostriatal fibers and cell bodies in the substantia nigra on the ipsilateral side in all the monkeys. The contralateral side showed variable reductions of TH-IR and AADC-IR staining in the striatum and the substantia nigra. AADC-IR staining paralleled TH-IR staining only in the AAV–LacZ-treated monkeys. The AAV–AADC-treated monkeys showed intense AADC staining in the ipsilateral striatum that exceeded staining
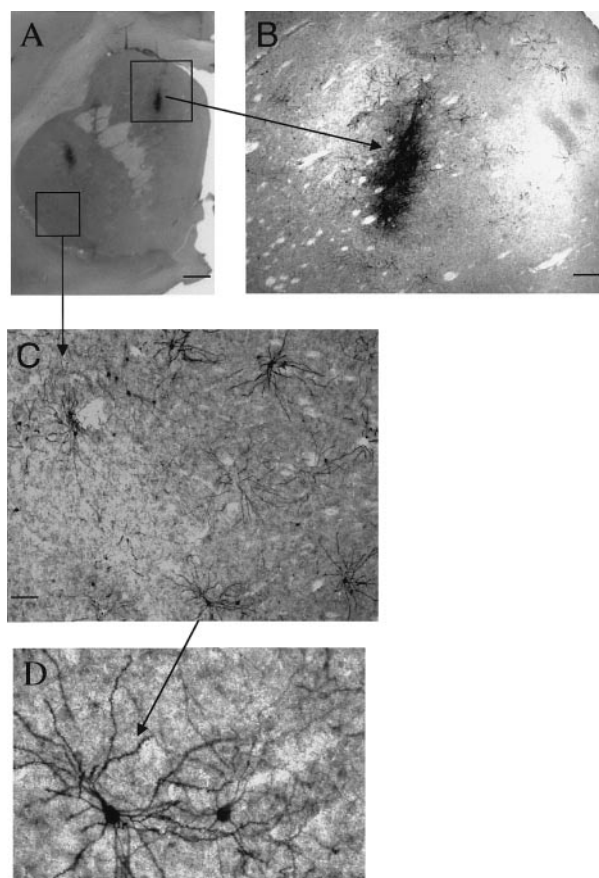

FIG. 4. Light microscopy view of LacZ-IR medium spiny neurons in AAV–LacZ-treated monkey (No. 6798). (A) Vector was administered using CED into the caudate nucleus and putamen. Fused silica tract is outlined in the box in the caudate nucleus and enlarged in Panel B. Region away from the cannula tract is outlined in the putamen and enlarged in Panel C. Scale bar = 1 mm. (B) Some LacZ-IR cells are present at the infusion site. Scale bar = 250 μm. (C) Majority of the AAV-infected cells are present away from the cannula tract following CED of AAV. Scale bar = 125 μm. (D) Almost all of the infected cells following AAV infection displayed morphology typical of a medium spiny neuron. Scale bar = 50 μm.
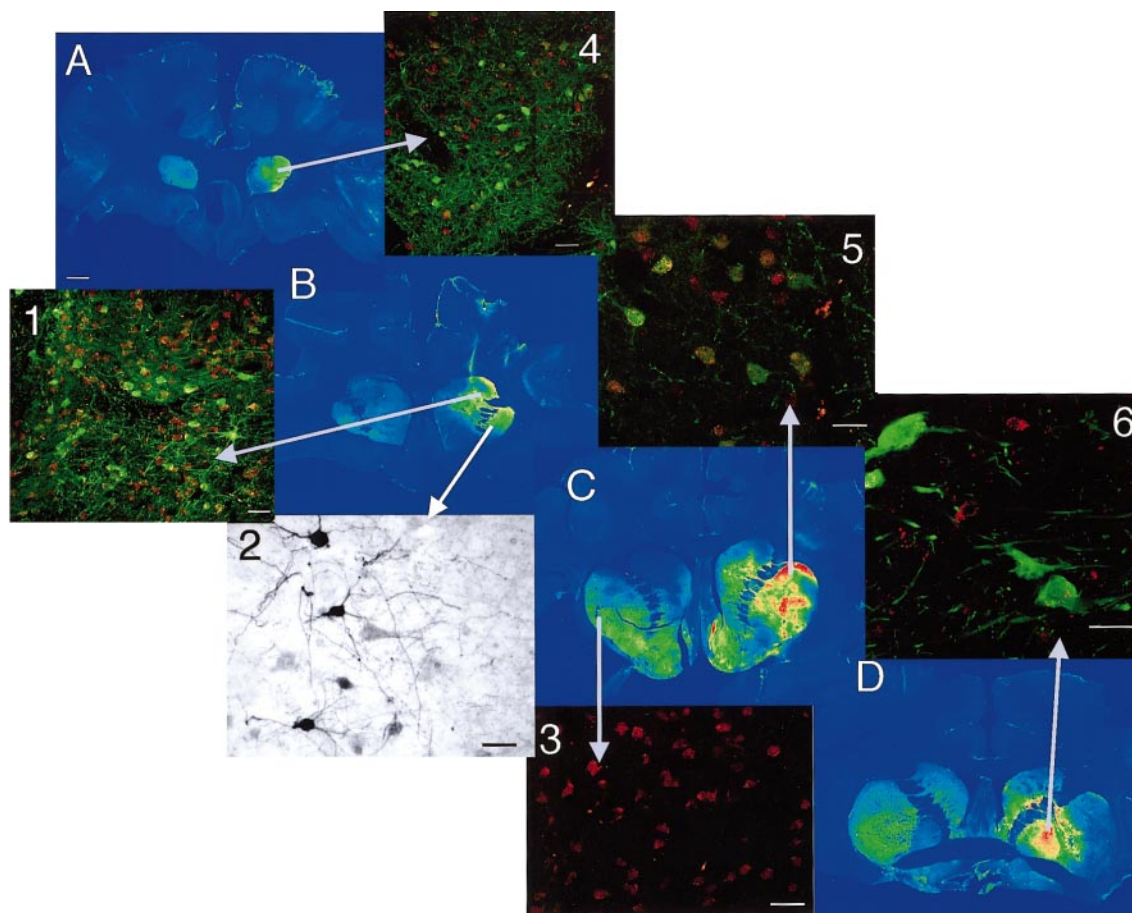
FIG. 5. AADC immunoreactivity (IR) of AAV–AADC-treated monkey (No. 6765) (1–6). The displayed sections represent the rostral-to-caudal extent of the striatum (A–D). AADC-IR cell bodies are present in the caudate and putamen over the entire striatum. In addition, the entire globus pallidus contains AADC-IR cell bodies (D). (1) Confocal view of the AADC-IR (green) and Neu-N-IR (red) cell bodies in the caudate (level B). All AADC-IR cells coexpressed Neu-N (red), strongly suggesting that AADC is mostly expressed in neurons. (2) Light microscopy view of AADC-IR cells in the putamen (level B). All of the cells displayed are positive; however, intensity of the staining might reflect a lower level of gene transfer. (3) Confocal view of the AADC-IR (green) and Neu-N (red) cell bodies in the contralateral putamen. No AADC-IR cells were found; only light fiber staining is present. (4) Confocal view of AADC-IR (green) and Neu-N-IR (red) neurons in the caudate nucleus (level A). (5) Confocal view of AADC-IR (green) and Neu-N-IR (red) neurons in the putamen (level C). Majority of the neurons at this level expressed AADC following AAV administration. (6) Confocal view of AADC-IR (green) and Neu-N-IR (red) neurons in the globus pallidus (level D). Scale bars: A–D = 3 mm, 1 and 4 = 50 μm; 2, 3, and 5 = 25 μm; 6 = 50 μm.

seen in the contralateral striatum (Fig. 2). There was a high density of AADC-IR cells throughout most of the striatum and globus pallidus of both monkeys and stereological analysis revealed many infected cells on the side of vector administration (Fig. 3). Robust LacZ IR staining was present in the caudate and putamen in monkeys treated with AAV–LacZ; however, there appeared to be a lower density of cells than in AAV–AADC-treated monkeys (Fig. 4). This is most likely due to the lower titer of AAV–LacZ than of AADC vector used in this experiment which can limit detection of gene expression by the immunostaining method (7). AAV-infected cells appeared to have a typical medium spiny neuron morphology and were markedly different than intrinsic TH-IR neurons (Fig. 4D). Infected cells were also positive for the neuronal marker Neu-N;

however, very few were GFAP-positive (data not shown), suggesting that the majority of expressing cells were neurons (Fig. 5).

To assess toxicity following AAV administration, areas adjacent to cannula tracts were stained with Nissl and H & E. Use of fused-silica cannula resulted in negligible needle tracts with almost no scar tissue. No signs of cytotoxicity and no perivascular cuffing were observed, regardless of the distance from the cannula (Fig. 6). The density of neurons was not reduced close to the infusion site when compared to the contralateral side as shown by Neu-N immunostaining. GFAP-immunostaining failed to detect any abnormal glial cells within the AAV-treated striatum. This lack of histological abnormalities confirmed the absence of adverse behavioral effects following AAV administration.
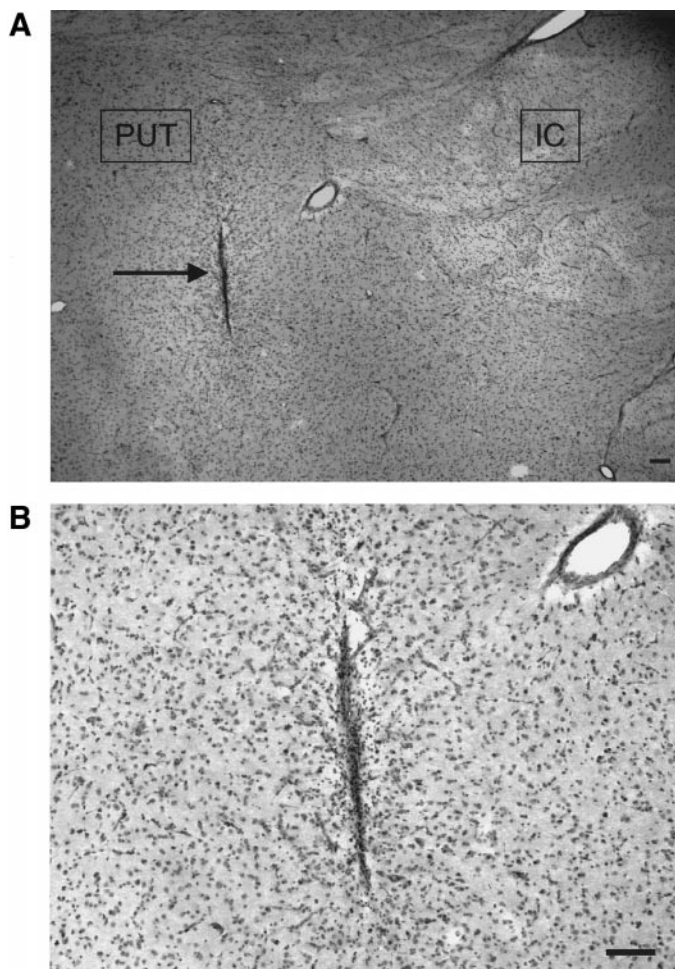
FIG. 6. Hematoxylin and eosin staining of the putamen following CED of AAV. (monkey 6765). (A) Low-power view showing fused silica cannula tract (arrow), internal capsule (IC), and the putamen (PUT). Please note several blood vessels in the vicinity and no evidence of perivascular cuffing and cellular infiltration. Scale bar = 250 μm. (B) Higher view of the fused silica cannula tract of the same region shown in Panel A. Scale bar = 250 μm.

To determine the biochemical outcome of AAV–AADC administration, tissue levels of L-dopa, dopamine, and HVA were examined following Sinemet treatment. Cortical regions in all monkeys showed variable levels of L-dopa; however, levels were consistent within each monkey (Fig. 5C). As expected, there was no decarboxylation of L-dopa to dopamine within the cortex. The L-dopa was converted to dopamine and further metabolized to HVA in the striatum on the side contralateral to MPTP administration (Fig. 7). In the ipsilateral MPTP-treated striatum of AAV–AADC-treated monkeys, L-dopa was converted to dopamine and HVA, and tissue levels of L-dopa in this region were greatly reduced (Fig. 7A). In the ipsilateral striatum of the AAV–LacZ monkeys, L-dopa was not converted to dopamine, nor was it metabolized to HVA, indicating a profound loss of AADC enzyme activity.

Tissue levels of L-dopa in the striatum also remained at the same levels as in the cortex in AAV–LacZ-treated monkeys, indicating that L-dopa was not converted to dopamine.

To quantify levels of AADC following AAV administration, tissue levels were measured by enzymatic assay. AADC activity was very low in the cortical regions of all of the monkeys and in the ipsilateral striatum of AAV–LacZ-treated monkeys. AADC activity in the ipsilateral striatum of AADC-treated monkeys, however, was restored to normal levels (Fig. 8). AADC activity was reduced in the contralateral striatum of all four monkeys in accordance with varying degrees of MPTP-induced lesions.

DISCUSSION

In this study, AADC delivery to the MPTP-treated striatum enabled the conversion of L-dopa to dopamine and subsequent metabolism to 3,4-dihydroxyphenylacetic acid (DOPAC) and homovanillic acid (HVA) by striatal neurons. Thus, there might be no need for incorporation of vesicular monoamine transporter-2 gene as shown by Lee *et al.* (24) in order to buffer unmetabolized L-dopa in the striatum. In addition, many of the AAV–AADC-infected striatal neurons most likely express D-1 and D-2 receptors. We believe that these cells, upon administration of L-dopa, will produce dopamine that might bind to cytoplasmic dopaminergic receptors (8, 32). Therefore, dopamine might not have to be released from the infected cells in order to bind to the dopaminergic receptors. Alternatively, if dopamine is released from the infected striatal neurons it will not have to diffuse far to bind to the extracytoplasmic dopaminergic receptors.

Conversion rates of L-dopa to dopamine following AADC gene transfer were as robust or greater than seen in the contralateral striatum (Figs. 7C and 2). A clear advantage of the AADC therapeutic approach to restoring dopaminergic activity is that only one gene has to be transfected and the regulation of dopamine levels is possible by controlling peripheral levels of L-dopa. To restore dopamine synthesis in the nigrostriatal pathway using a gene transfer approach, expression of three genes would need to be achieved. The genes for TH, for TH co-factor tetrahydrobiopterin (GTP-cyclohydroxylase-1), and for AADC would all have to be successfully expressed to synthesize dopamine *in situ* (14, 19, 28, 35). In addition to the problems associated with delivering three genes at appropriate levels, the regulation of dopamine levels would be difficult to control using this approach. By delivering only AADC gene, L-dopa can be used as a pro-drug to regulate dopamine levels in the striatum (11).

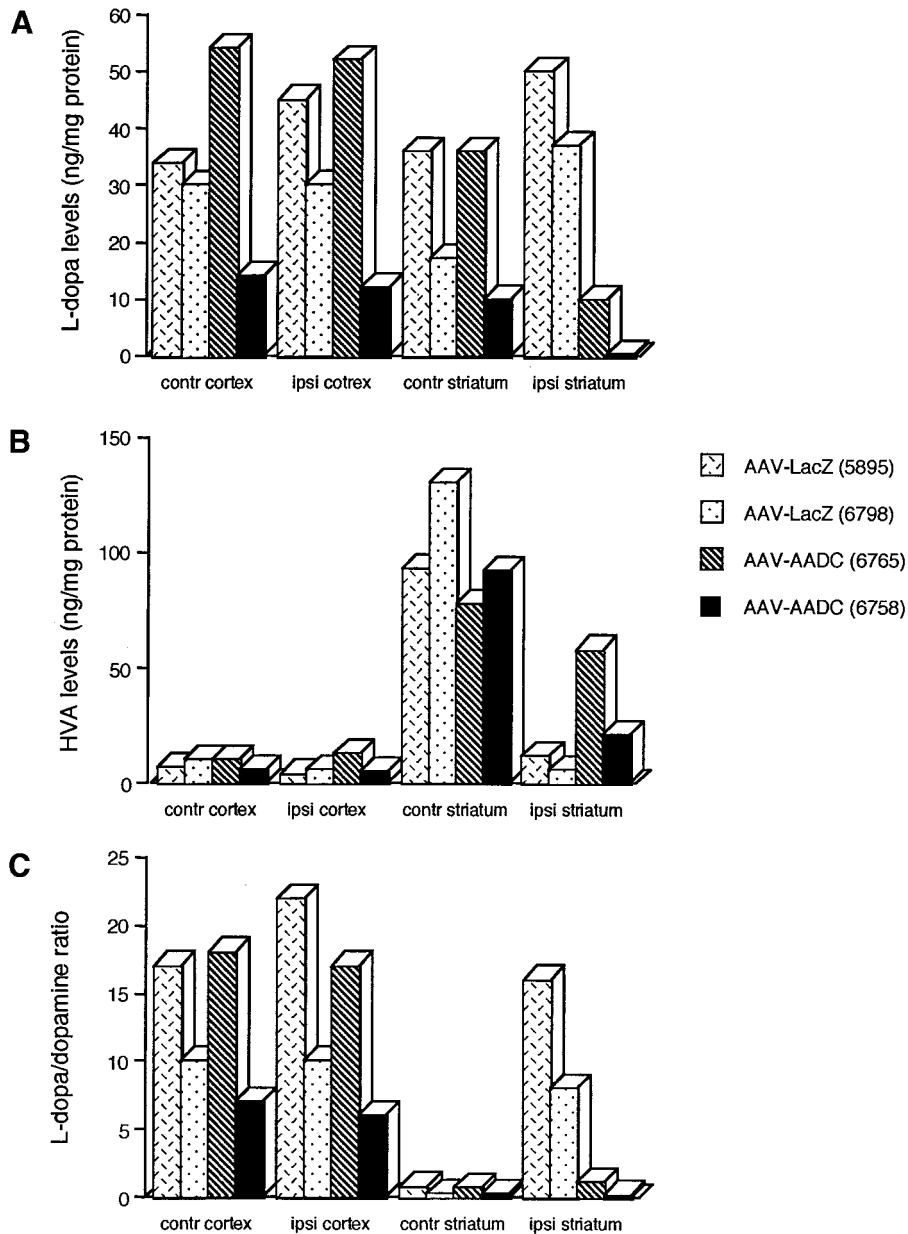The progressive loss of striatal dopaminergic nerve terminals in idiopathic Parkinson's disease is respon-

FIG. 7. Biochemical consequences of L-dopa/carbidopa administration following AAV–AADC gene transfer. (A) L-dopa levels were measured in the tissue punches following L-dopa/carbidopa administration. Due to differences in L-dopa absorption, tissue levels varied between monkeys but were similar within each animal. Tissue levels of L-dopa were dramatically reduced in the ipsilateral striatum of AAV–AADC-treated monkeys since the AADC enzyme was restored and the L-dopa was converted to dopamine and subsequently HVA (see Panel B). In fact, L-dopa levels were lower than those in the contralateral striatum in these animals. In the AAV–LacZ-treated animals L-dopa levels in the ipsilateral striatum were significantly higher than those in the contralateral striatum. (B) HVA is a metabolite of dopamine catabolism. Since cortical regions are unable to convert L-dopa to dopamine, HVA levels are low. As shown in Panel A, the striatum converts L-dopa to dopamine; dopamine is normally catabolized to HVA in this region. HVA levels were low in the ipsilateral striatum of the AAV–LacZ-treated monkeys due to the near complete depletion of AADC by MPTP (see Fig. 8). AAV–AADC-treated animals in which ipsilateral striatal AADC activity was restored showed nearly normal HVA levels. (B, C) L-Dopa is converted to dopamine by the AADC enzyme. In cortical regions, regardless of MPTP treatment, there is poor or no conversion of L-dopa to dopamine. The striatum is AADC-rich, and, therefore, L-dopa is almost entirely converted to dopamine in this region. Following administration of L-dopa, AAV–LacZ-treated monkeys showed similar L-dopa to dopamine conversion rates in the ipsilateral (side of ICA MPTP infusion) striatum and cortex due to the depletion of AADC in the ipsilateral striatum. In contrast, both AAV–AADC-treated animals show nearly normal L-dopa to dopamine conversion rates in the ipsilateral striatum.
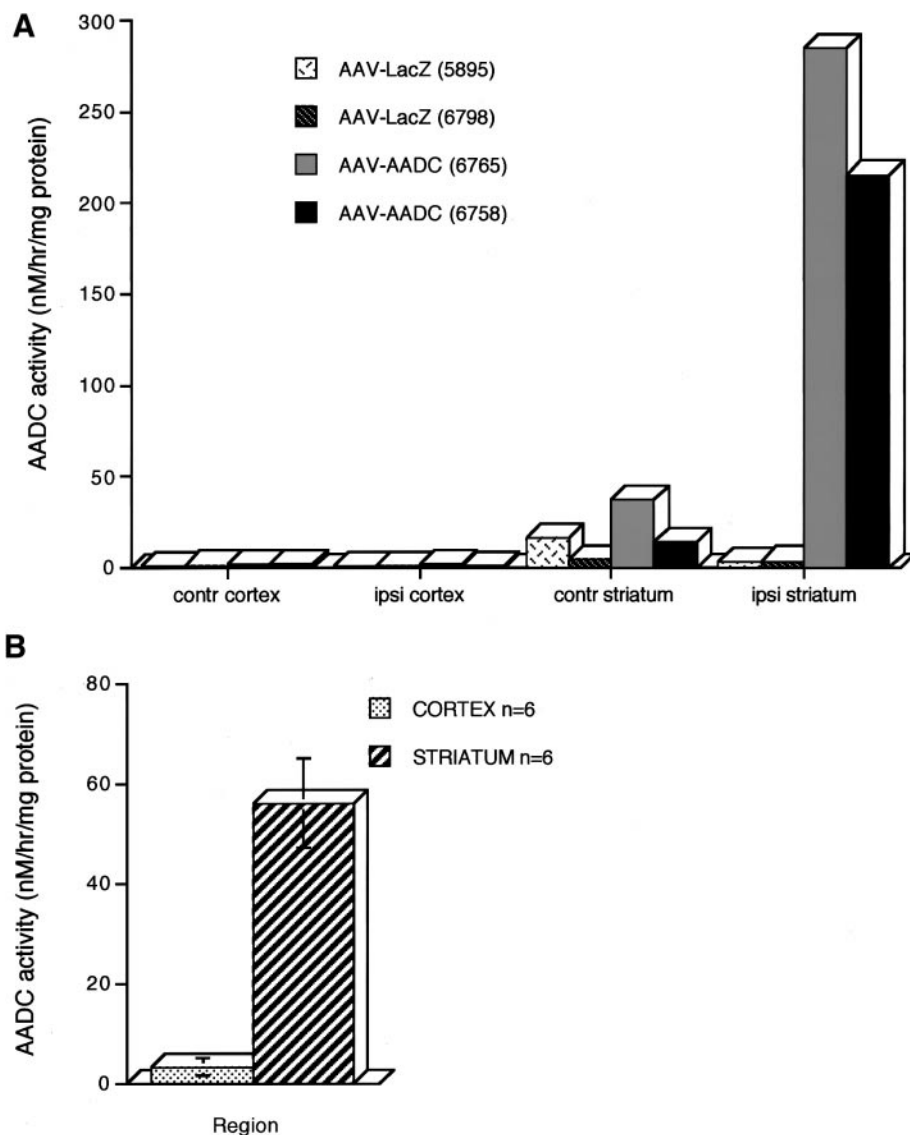
FIG. 8. Activity of the AADC enzyme *in vitro* in animals subjected to gene therapy (A) and control naive rhesus monkeys (B). Tissue punches were incubated with L-dopa (see Materials and Methods). (A) As expected, cortical regions contained low levels of AADC. AADC activity was relatively high in the contralateral striatum for all monkeys, although levels varied with the degree of the partial lesion on that side of the brain. AADC activity was significantly reduced in the ipsilateral striatum for the AAV–Lac-Z-treated monkeys but was restored to levels that were three to four times greater than normal levels (see Panel B) in the AAV–AADC-treated monkeys. (B) AADC enzyme activity measured in naïve rhesus monkeys. Tissue was processed together with that of the gene therapy-treated monkeys and it is shown for comparison (±SD). AADC activity is expressed as nM/h/mg of protein.

sible for clinical deterioration. One of the most important aspects of the degenerative process is reduced clinical response to L-dopa/carbidopa treatment. Typically, patients in early stages of the disease respond well to this treatment with very few side effects and a long therapeutic response per dose. However, as the disease progresses, patients typically require increasingly higher doses of L-dopa/carbidopa, more side effects occur, and the therapeutic response becomes shorter. It is possible that, in addition to receptor failure, further depletion of the nigrostriatal pathway that serves as the site for L-dopa decarboxylation to dopa-

mine and storage of unmetabolized dopamine is responsible for the collapse of the therapeutic window (27, 29, 31). We postulate here that AAV-mediated restoration of both AADC activity and dopamine storage within infected striatal neurons might restore the therapeutic window, thereby providing patients with a potentially better response to L-dopa/carbidopa.

Degeneration of the dopaminergic system in patients with idiopathic Parkinson's disease is not uniform. The nigrostriatal pathway degenerates much faster than the mesolimbic pathway, leaving patients with an imbalance between the activity of the two pathways (15).

As the disease progresses, higher levels of L-dopa are needed to compensate for nigrostriatal degeneration, but this also results in increasingly higher dopamine levels in the nucleus accumbens and other parts of the mesolimbic system. Such overproduction may be responsible for some of the side effects, such as hallucinations, associated with L-dopa treatment. Similarly, MPTP leaves the mesolimbic dopaminergic system relatively spared (see Figs. 2A-1 and 2B-1, no dopaminergic innervation is present in the caudate and putamen; a partial lesion is seen in the nucleus accumbens). As seen in Figs. 2C-1 and 2D-1, AAV–AADC can restore this imbalance. Therefore, it is possible that lower doses of L-dopa will be required following restoration of AADC enzyme levels and improved L-dopa to dopamine conversion rates. This in turn might reduce overstimulation of the mesolimbic system, resulting in fewer L-dopa/carbidopa-related side effects.

An important aspect of this work is the demonstration of gene transfer *in vivo.* The AADC tracer, FMT, is both decarboxylated and stored in striatal neurons of MPTP-treated monkeys providing a method for *in vivo* visualization of gene transfer in the brain. This method can be applied to many vector systems other than AAV that can infect cells *in vivo.* In addition, grafting AADC gene-transfected cells *ex vivo* into the striatum of MPTP-treated monkeys may enable evaluation of graft survival and persistence of gene expression. This *in vivo* system of gene transfer detection is possible because MPTP significantly depletes not only TH but also AADC and dopamine storage sites in the nigrostriatal fibers (Figs. 2A and 2B). Following restoration of AADC activity by gene transfer, gene expression levels can be monitored over time to determine the long-term performance of the vector system used. The PET findings presented here correlate well with the postmortem findings, indicating that PET–FMT studies should be useful for determining the extent of gene delivery and expression. Additionally, since AAV is capable of long-term gene transfer (25) sequential PET–FMT studies could be performed to evaluate gene regulation *in vivo* using vectors with regulated promoters.

In this study we demonstrated that a fundamental obstacle in the gene therapy approach to the central nervous system (CNS), i.e., the ability to deliver viral vectors in sufficient quantities to the brain, can be overcome by using CED. In direct comparison between CED and simple injection of AAV in MPTP-treated monkeys we found a significant increase of gene transfer following the CED method (3, 4, 7). Here we showed that AAV can be safely distributed over the whole anatomical target region of a monkey brain using the CED method. The results predict the potential of efficient and optimal gene delivery that can be translated to the size of a human brain. This in itself demonstrates a realistic opportunity for the delivery of therapeutic agents to CNS by gene therapy. Ongoing studies are evaluating the clinical efficacy of this approach.

REFERENCES

1. Bankiewicz, K. S., E. H. Oldfield, C. C. Chiueh, J. L. Doppman, D. M. Jacobowitz, and I. J. Kopin. 1986. Hemiparkinsonism in monkeys after unilateral internal carotid artery infusion of 1-methyl-4-phenyl-1,2,3,6-tetrahydropyridine (MPTP). *Life Sci.* **39:** 7–16.

2. Bankiewicz, K. S., R. Sanchez-Pernaute, Y. Oiwa, M. Kohutnicka, A. Cummins, and J. L. Eberling. (1999). *Curr. Protocols Neurosci.* 9.4.1–9.4.32.

3. Bankiewicz, K. S., R. Snyder, S. Z. Zhou, M. Morton, J. Conway, and D. Nagy. 1996. Adeno-associated (AAV) viral vector-mediated gene delivery in non-human primates. *Soc. Neurosci. Abstr.* **22:** 768.

4. Bankiewicz, K. S., S. Leff, D. Nagy, S. Jungles, J. Rokovich, K. Spratt, L. Cohen, M. Libonati, O. Richard, R. O. Snyder, and R. Mandel. 1997. Practical aspects of the development of *ex vivo* and *in vivo* gene therapy for Parkinson's disease. *Exp. Neurol.* **144**(1): 147–156.

5. Birkmayer, W., and O. Hornykiewicz. 1961. In *Wien Klin Worchenchr,* Vol. 73, pp. 787–792. Springer-Verlag, Berlin.

6. Cavalieri, B. 1966. In *Geometric degl: Indivisible,* pp. 1–543. Unione Tipografico, Editrice, Torino.

7. Cunningham, J., Y. Oiwa, D. Nagy, G. Podsakoff, P. Colosi, and K. S. Bankiewicz. 2000. Distribution of AAV-TK following intracranial convection-enhanced delivery into rats. *Cell Transplant.,* in press.

8. Dumartin, B., I. Caille, F. Gonon, and B. Bloch. 1998. Internalization of D1 dopamine receptor in striatal neurons in vivo as evidence of activation by dopamine agonists. *J. Neurosci.* **18:** 1650–1661.

9. During, M. J., J. R. Naegele, K. L. O'Malley, and A. I. Geller. 1994. Long-term behavioral recovery in parkinsonian rats by an HSV vector expressing tyrosine hydroxylase. *Science* **266:** 1399–1403.

10. During, M. J., R. J. Samulski, J. D. Elsworth, M. G. Kaplitt, P. Leone, X. Xiao, J. Li, A. Freese, J. R. Taylor, R. H. Roth, J. R. Sladek, Jr., K. L. O'Malley, and D. E. Redmond, Jr. 1998. In vivo expression of therapeutic human genes for dopamine production in the caudates of MPTP-treated monkeys using an AAV vector. *Gene Ther.* **5:** 820–827.

11. Eberling, J. L., E. O. Major, D. Nagy, and K. S. Bankiewicz. 1998. *Genetic Engineering for Parkinson's disease: CNS Regeneration. Basic Science and Clinical Advances.* Academic Press, San Diego.

12. Eberling, J. L., K. S. Bankiewicz, P. Pivirotto, J. Bringas, K. Chen, D. P. Nowotnik, J. P. Steiner, T. F. Budinger, and W. J. Jagust. 1999. Dopamine transporter loss and clinical changes in MPTP-lesioned primates. *Brain Res.* **832:** 184–187.

13. Eberling, J. L., W. J. Jagust, S. Taylor, J. Bringas, P. Pivirotto, H. F. VanBrocklin, and K. S. Bankiewicz. 1998. A novel MPTP primate model of Parkinson's disease: Neurochemical and clinical changes. *Brain Res.* **805:** 259–262.

14. Fan, D. S., M. Ogawa, K. I. Fujimoto, K. Ikeguchi, Y. Ogasawara, M. Urabe, M. Nishizawa, I. Nakano, M. Yoshida, I.

Nagatsu, H. Ichinose, T. Nagatsu, G. J. Kurtzman, and K. Ozawa. 1998. Behavioral recovery in 6-hydroxydopamine-lesioned rats by cotransduction of striatum with tyrosine hydroxylase and aromatic L-amino acid decarboxylase genes using two separate adeno-associated virus vectors. *Hum. Gene Ther.* **9:** 2527–2535.

15. Gibb, W. R., and A. J. Lees. 1991. Anatomy, pigmentation, ventral and dorsal subpopulations of the substantia nigra, and differential cell death in Parkinson's disease. *J. Neurol. Neurosurg. Psychiatry* **54:** 388–396.

16. Herzog, R. W., E. Y. Yang, L. B. Couto, J. M. Hagstrom, D. Elwell, P. A. Fields, M. Burton, D. A. Bellinger, M. S. Read, K. M. Brinkhous, G. Podsakoff, T. C. Nichols, G. J. Kurtzman, and K. A. High. 1999. Long-term correction of canine hemophilia B by gene transfer of blood coagulation factor IX mediated by adeno associated viral vector. *Nat. Med.* **5:** 56–63.

17. Jordan, S., J. L. Eberling, K. S. Bankiewicz, D. Rosenberg, P. G. Coxson, H. F. VanBrocklin, J. P. O'Neil, M. E. Emborg, and W. J. Jagust. 1997. 6-[18F]fluoro-L-*m*-tyrosine: Metabolism, PET kinetics, and MPTP lesions in primates. *Brain Res.* **750:** 264–276.

18. Jordan, S., K. S. Bankiewicz, J. L. Eberling, H. F. VanBrocklin, J. P. O'Neill, and W. J. Jagust. 1998. An in vivo microdialysis study of striatal 6-[18F]fluoro-L-*m*-tyrosine metabolism. *Neurochem. Res.* **23:** 513–517.

19. Kang, U. J., C. Bencsics, S. Wachtel, and R. Lew. 1998. The effect of GTP cyclohydrolase-1 on tyrosine hydroxylase expression: Implications in DOPA-responsive dystonia. *Adv. Neurol.* **78:** 319–324.

20. Kaplitt, M. G., A. D. Kwong, S. P. Kleopoulos, C. V. Mobbs, S. D. Rabkin, and D. W. Pfaff. 1994. Preproenkephalin promoter yields region-specific and long-term expression in adult brain after direct in vivo gene transfer via a defective herpes simplex viral vector. *Proc. Natl. Acad. Sci. USA* **91:** 8979–8983.

21. Kaplitt, M. G., P. Leone, R. J. Samulski, X. Xiao, D. W. Pfaff, and K. L. O'Malley. 1994. Long-term gene expression and phenotypic correction using adeno-associated virus vectors in the mammalian brain. *Nat. Genet.* **8:** 148–154.

22. Kordower, J. H., J. Bloch, S. Y. Ma, Y. Chu, S. Palfi, B. Z. Roitberg, M. Emborg, P. Hantraye, N. Deglon, and P. Aebischer. 1999. Lentiviral gene transfer to the nonhuman primate brain. *Exp. Neurol.* **160:** 1–16.

23. Kordower, J. H., S. Palfi, E. Y. Chen, S. Y. Ma, T. Sendera, E. J. Cochran, E. J. Mufson, R. Penn, C. G. Goetz, and C. D. Comella. 1999. Clinicopathological findings following intraventricular glial-derived neurotrophic factor treatment in a patient with Parkinson's disease. *Ann. Neurol.* **46:** 419–424.

24. Lee, W. Y., J. W. Chang, N. L. Nemeth, and U. J. Kang. 1999. Vesicular monoamine transporter-2 and aromatic L-amino acid decarboxylase enhance dopamine delivery after L-3,4-dihydroxyphenylalanine administration in parkinsonian rats. *J. Neurosci.* **19:** 3266–3274.

25. Leff, S. E., S. K. Spratt, R. O. Snyder, and R. J. Mandel. 1999. Long-term restoration of striatal L-aromatic amino acid decarboxylase activity using recombinant adeno-associated virus in

an animal model of Parkinson's disease. *Neuroscience* **92:** 187–198.

26. Lieberman, D. M., D. W. Laske, P. F. Morrison, K. S. Bankiewicz, and E. H. Oldfield. 1995. Convection-enhanced distribution of large molecules in gray matter during interstitial drug infusion. *J. Neursurg.* **82:** 1021–1029.

27. Lloyd, K. G., L. Davidson, and O. Hornykiewicz. 1975. The neurochemistry of Parkinson's disease: Effect of L-dopa therapy. *J. Pharmacol. Exp. Ther.* **195:** 435–446.

28. Mandel, R. J., K. G. Rendahl, S. K. Spratt, R. O. Snyder, L. K. Cohen, and S. E. Leff. 1998. Characterization of intrastriatal recombinant adeno-associated virus-mediated gene transfer of human tyrosine hydroxylase and human GTP-cyclohydrolase I in a rat model of Parkinson's disease. *J. Neurosci.* **18:** 4271–4284.

29. Marsden, C. D., and J. D. Parkes. 1977. Success and problems of long-term levodopa therapy in Parkinson's disease. *Lancet* **1:** 345–349.

30. Matsushita, T., S. Elliger, C. Elliger, G. Podsakoff, L. Villarreal, G. J. Kurtzman, Y. Iwaki, and P. Colosi. 1998. Adeno-associated virus vectors can be efficiently produced without helper virus. *Gene Ther.* **5:** 938–945.

31. Mouradian, M. M., J. L. Juncos, G. Fabbrini, and T. N. Chase. 1987. Motor fluctuations in Parkinson's disease: Pathogenic and therapeutic studies. *Ann. Neurol.* **22:** 475–479.

32. Muriel, M. P., V. Bernard, A. I. Levey, O. Laribi, D. N. Abrous, Y. Agid, B. Bloch, and E. C. Hirsch. 1999. Levodopa induces a cytoplasmic localization of D1 dopamine receptors in striatal neurons in Parkinson's disease. *Ann. Neurol.* **46:** 103–111.

33. Nagatsu, T., T. Yamamoto, and T. Kato. 1979. A new and highly sensitive voltammetric assay for aromatic L-amino acid decarboxylase activity by high-performance liquid chromatography. *Anal. Biochem.* **100:** 160–165.

34. Neff, N. H., and M. Hadjiconstantinou. 1995. Aromatic L-amino acid decarboxylase modulation and Parkinson's disease. *Prog. Brain Res.* **106:** 91–97.

35. Szczypka, M. S., R. J. Mandel, B. A. Donahue, R. O. Snyder, S. E. Leff, and R. D. Palmiter. 1999. Viral gene delivery selectively restores feeding and prevents lethality of dopamine-deficient mice. *Neuron* **22:** 167–178.

36. Valk, P. E., W. J. Jagust, S. E. Derenzo, R. H. Huesman, A. B. Geyer, and T. F. Budinger. 1990. Clinical evaluation of a high resolution (2.6-mm) positron emission tomography. *Radiology* **176:** 783–790.

37. Wang, J., R. Saunders, T. Aigner, J. Hsio, and K. S. Bankiewicz. 1990. Methodology of microdialysis of neostraiatum in hemiparkinsonian nonhuman primates. *Exp. Neurol.* **110:** 181–186.

38. West, M. J., K. Ostergaard, O. A. Andreassen, and B. Finsen. 1996. Estimation of the number of somatostatin neurons in the striatum: An in situ hybridization study using optical fractionator method. *J. Comp. Neurol.* **370:** 11–22.

39. Wigler, M., M. Perucho, D. Kurtz, S. Dana, A. Pellicer, R. Axel, and S. Silverstein. 1980. Transformation of mammalian cells with an amplifiable dominant-acting gene. *Proc. Natl. Acad. Sci. USA* **77:** 3567–3570.